ADVANCED MATERIALS
www.advmat.de

Colloidal Nanosurfactants for 3D Conformal Printing of 2D van der Waals Materials

*Minxiang Zeng, Wenzheng Kuang, Irfan Khan, Dali Huang, Yipu Du, Mortaza Saeidi-Javash, Lecheng Zhang, Zhengdong Cheng, Anthony J. Hoffman, and Yanliang Zhang**

Printing techniques using nanomaterials have emerged as a versatile tool for fast prototyping and potentially large-scale manufacturing of functional devices. Surfactants play a significant role in many printing processes due to their ability to reduce interfacial tension between ink solvents and nanoparticles and thus improve ink colloidal stability. Here, a colloidal graphene quantum dot (GQD)-based nanosurfactant is reported to stabilize various types of 2D materials in aqueous inks. In particular, a graphene ink with superior colloidal stability is demonstrated by GQD nanosurfactants via the π–π stacking interaction, leading to the printing of multiple high-resolution patterns on various substrates using a single printing pass. It is found that nanosurfactants can significantly improve the mechanical stability of the printed graphene films compared with those of conventional molecular surfactant, as evidenced by 100 taping, 100 scratching, and 1000 bending cycles. Additionally, the printed composite film exhibits improved photoconductance using UV light with 400 nm wavelength, arising from excitation across the nanosurfactant bandgap. Taking advantage of the 3D conformal aerosol jet printing technique, a series of UV sensors of heterogeneous structures are directly printed on 2D flat and 3D spherical substrates, demonstrating the potential of manufacturing geometrically versatile devices based on nanosurfactant inks.

Solution-based processing of nanomaterials has been studied recently as an emerging technique to complement the semiconductor industry owing to its rapid customization and the ability to fabricate wearable/flexible devices.[1] Compared with conventional solution-processing methods (e.g., spin coating), noncontact printing strategies (e.g., inkjet printing and aerosol jet printing) provide technological avenues to directly convert nanoparticles into final device patterns on both 2D and 3D substrates with superior spatial resolution (line width of approximately 10 µm), which is essential for fabricating microscale devices with sophisticated architectures.[2] A wide range of functional devices, including sensors,[3] thermoelectrics,[4] and energy storage devices,[5] have been developed by printing colloidal nanomaterials. Recently, 2D nanomaterials have garnered research interests owing to their promising electronic/optical properties.[6–9] For example, flexible thin-film transistors printed with 2D nanomaterials inks including graphene (Gr), transition metal dichalcogenide (TMD), and hexagonal boron nitride (h-BN) have been demonstrated.[10] In the past decade, organic solvents including ethanol, cyclohexanone, terpineol, and ethylene glycol have been extensively investigated for the printing of 2D nanomaterials;[4,5] however, limitations of organic solvents still exist due to their inherent toxicity, flammability, and poor biocompatibility. To manufacture functional devices in a scalable, sustainable, and affordable manner, conventional ink formulations that involve toxic/expensive organic solvents should be avoided, mandating the need for a new generation of water-based nanoparticle inks.

To formulate printable 2D nanomaterial inks in water, organic surfactants (either polymers or small-molecule amphiphiles) are often required to suppress particle aggregation.[6] These organic molecules can reduce the surface tension of water as well as the interfacial energy of particles and water, improving the colloidal stability of nanoparticle inks.[11] Several surfactants have been reported to stabilize 2D nanosheets, while discotic amphiphiles (e.g., sodium cholate (SC)) are particularly effective for dispersing 2D nanomaterials.[12] Due to effective adsorptions on the surface of 2D flakes, SC has demonstrated good surfactant properties in stabilizing aqueous dispersions of WS_2, $MoSe_2$, $MoTe_2$, and h-BN nanoplates.[13] Despite significant advances in surfactant-based ink formulation, several challenges still exist. For example, conventional

Dr. M. Zeng, W. Kuang, Y. Du, M. Saeidi-Javash, Prof. Y. Zhang
Department of Aerospace and Mechanical Engineering
University of Notre Dame
Notre Dame, IN 46556, USA
E-mail: yzhang45@nd.edu
I. Khan, Prof. A. J. Hoffman
Department of Electrical Engineering
University of Notre Dame
Notre Dame, IN 46556, USA
D. Huang, Dr. L. Zhang, Prof. Z. Cheng
Artie McFerrin Department of Chemical Engineering
Texas A&M University
College Station, TX 77843, USA
Prof. Z. Cheng
Chemical Engineering Department
Texas A&M University at Qatar
P.O. Box 23874, Doha, Qatar
The ORCID identification number(s) for the author(s) of this article can be found under https://doi.org/10.1002/adma.202003081.

DOI: 10.1002/adma.202003081

surfactants have limited or no contribution to the mechanical bonding of printed nanomaterials, and thus additional polymer binders are required to print robust devices.[14,15] Even worse, the residual of organic surfactants in printed devices often compromises the overall functionalities of nanomaterials (e.g., deteriorating interfacial transport properties), which requires severe post-treatments such as high-temperature thermal annealing or expensive laser sintering.[16–19] Therefore, the development of new surfactants that may not compromise or may even improve the performance of printed devices is essential for the printing of next-generation high-performance devices.

Nanoparticle-based surfactants or so-called nanosurfactants (NanoSs) have emerged as a new category of surfactants due to the unique synergetic behavior of nanoparticles and surfactants.[20,21] In these surfactants, nanoparticles are engineered with functional groups on the surface via either electrostatic forces or covalent bonding, which render their ability of reducing the interfacial tension as well as stabilizing various colloidal systems.[21–23] Recently, studies on Pickering emulsions have shown that graphene,[24] MoS_2,[25] aluminosilicate clays,[26,27] and some quantum dots (QDs)[28] are able to lower interfacial tension and show "surfactancy" upon appropriate design of their surface properties. These nanoparticle-based surfactants retain their nanoparticle properties (e.g., electronic bandgap), which could be beneficial in overall device performance, eliminating the need of surfactant removal for final device fabrication. For example, graphene showed weak photoconductance because of the ultrafast recombination of photocarriers,[29,30] which makes it challenging to be directly used in optical detectors; yet the viability of graphene in such applications could be improved using nanosurfactants with suitable bandgap. The judicious use of nanosurfactant in ink formulations may circumvent the inherent limitation of molecular surfactants; however, nanosurfactants have rarely been explored in additive manufacturing and their printing behavior in device fabrication remains largely unknown.

Here, we report a highly versatile water-based ink formulation with surface-active nanosurfactants of graphene QD (GQD) for printing a range of 2D materials. During the ink formulation, colloidal NanoS is used to directly exfoliate 2D van der Waals crystals into few-layer nanosheets in aqueous dispersion (Figure S1, Supporting Information). Taking graphene ink as an example, the colloidal NanoS is able to generate electrostatic stabilization for the graphene flakes, while no organic surfactant or polymer binder is introduced in inks. Due to the polyaromatic core structure, the graphene QD exhibits noncovalent π–π interactions with graphene (**Figure 1**a), leading to long-term improvement in colloidal stability of graphene inks. The transmission electron microscopy (TEM) analysis of graphene inks confirms the noncovalent adsorption of NanoS particles accumulated on graphene nanosheets (Figure 1b). The π–π stacking force between graphene and NanoS is a reminiscent of the interaction of graphene with small-molecule pyrene sulfonic acid sodium salt (PSA), which has been widely used in liquid exfoliation of few-layer graphene in water.[31,32] Remarkably, such QD nanosurfactant can facilitate exfoliation and stabilization of several 2D nanosheets from their bulk layered crystals, including zero-bandgap graphene, medium-bandgap TMD (MoS_2 and WS_2), and large-bandgap h-BN, as shown in Figure 1c. The interfacial tension measurement of water/dodecane system shows that the NanoS, similar to molecular surfactants, can effectively reduce the interfacial tension of water phase (Figure 1d; Figure S2, Supporting Information). Moreover, we found that the NanoS, in addition to stabilizing

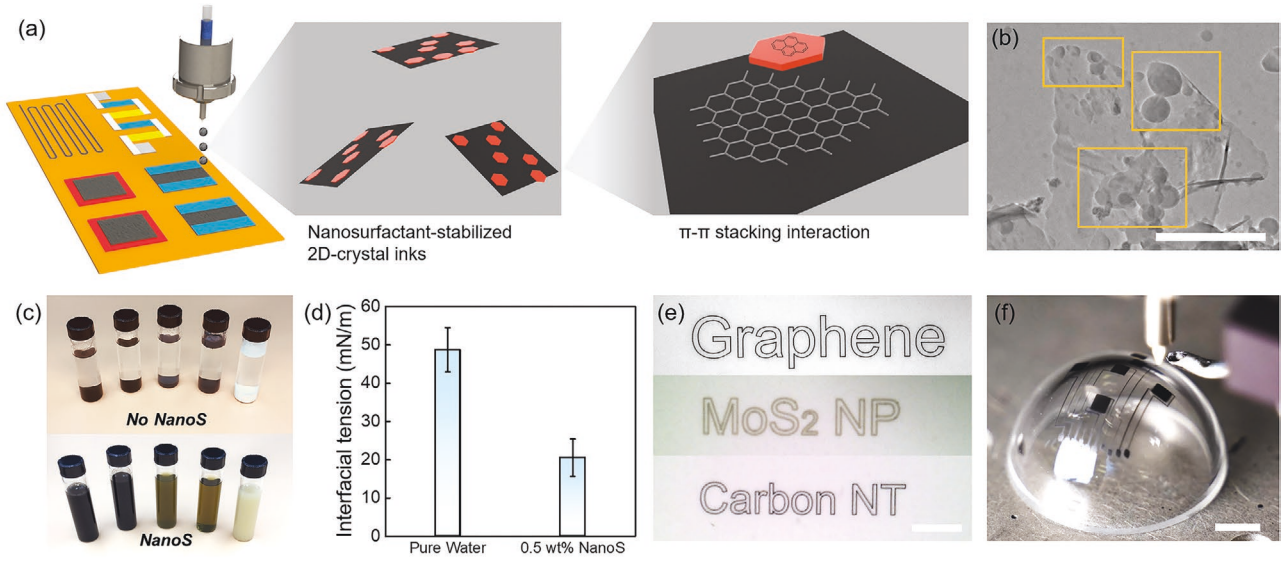

Figure 1. Nanosurfactant-stabilized 2D material inks and their properties. a) Schematic illustration of printing graphene ink using QD-based nanosurfactant as the dispersant. b) TEM image of NanoS-stabilized graphene nanosheets. Scale bar is of 500 nm. c) Camera images of various 2D-crystal inks with and without nanosurfactant. The nanoparticle inks from left to right are graphene, carbon nanotubes, WS_2, MoS_2, and h-BN. d) Reduced interfacial tension of water/dodecane system by introducing NanoS. e) The printed patterns of "Graphene," "MoS_2 NP," and "Carbon NT" using water-based graphene, MoS_2, and carbon nanotube ink, respectively. Scale bar is of 2 mm. f) Photographic demonstration of 3D conformal printing process using an aerosol jet printer. Scale bar is of 5 mm.

2D nanomaterials, can alleviate the aggregation of 1D carbon nanotubes (NTs) in water (Figure 1c). While pristine particles without NanoS stabilization tend to aggregate and sediment in a few hours (Figure 1c top), these 2D flakes and 1D nanotubes with NanoS were proven to be highly colloidal stable in water (up to months), and showed high zeta potential values (detailed discussion on colloidal stability of NanoS-based inks can be found in Figures S3–S7 in the Supporting Information). Figure 1e shows some examples of printed patterns obtained with water-based inks including graphene, MoS_2, and carbon nanotubes inks on paper substrates. Among those stabilized nanoparticle inks, graphene and carbon nanotubes showed a higher particle concentration than MoS_2 and WS_2 under the same exfoliation condition (Figure S4, Supporting Information). This is due to that graphene and carbon nanotubes both contain sp^2 carbon structures that can form noncovalent π–π bonding with QD NanoS, whereas MoS_2 and WS_2 are transition metal chalcogenides without free π electrons and thus interact with NanoS via only van der Waals force. These results are comparable with the molecular counterparts, such as PSA or SC surfactant.[13,33] Due to the high colloidal stability of 2D crystal inks, a 3D conformal pattern can be readily printed, as shown in Figure 1f.

To understand how the nanosurfactants affect the printing process, we systematically studied the printing performance of NanoS-stabilized graphene inks. As shown in **Figure 2**a and Figures S8 and S9 in the Supporting Information, the printed graphene patterns on various substrates (SiO_2, polyimide, and glass) exclusively show good continuity and uniformity without an observable coffee-ring effect. The printing behaviors of NanoS-stabilized graphene inks were investigated by varying several printing parameters (e.g., flow rate of ink aerosol, flow rate of sheath gas, and printing speed), revealing on-demand control of the line width from ≈15 to 50 µm (see Figure S8 in the Supporting Information). Such smooth printing of NanoS-based inks further confirms the high colloidal stability of the ink, where no disadvantageous particle aggregation is observed. Compared with inkjet printing techniques requiring relatively low ink viscosity (normally <30 mPa s),[34,35] our aerosol jet printing can tolerate ink viscosity ranging from 1 mPa s to around 2500 mPa s, enabling high particle loading without ink clogging during printing. One advantage of high-concentration inks is the rapid fabrication of thick and dense films for only a few print passes, significantly saving the printing time in device fabrication. As shown in Figure 2b, the thickness of the printed film increases as a function of print passes, with each additional pass adding 1228 ± 44 nm before annealing, or 921 ± 102 nm after thermal annealing. While some graphene films involving molecular surfactant were reported to show 50–80% thickness reduction during annealing processes due

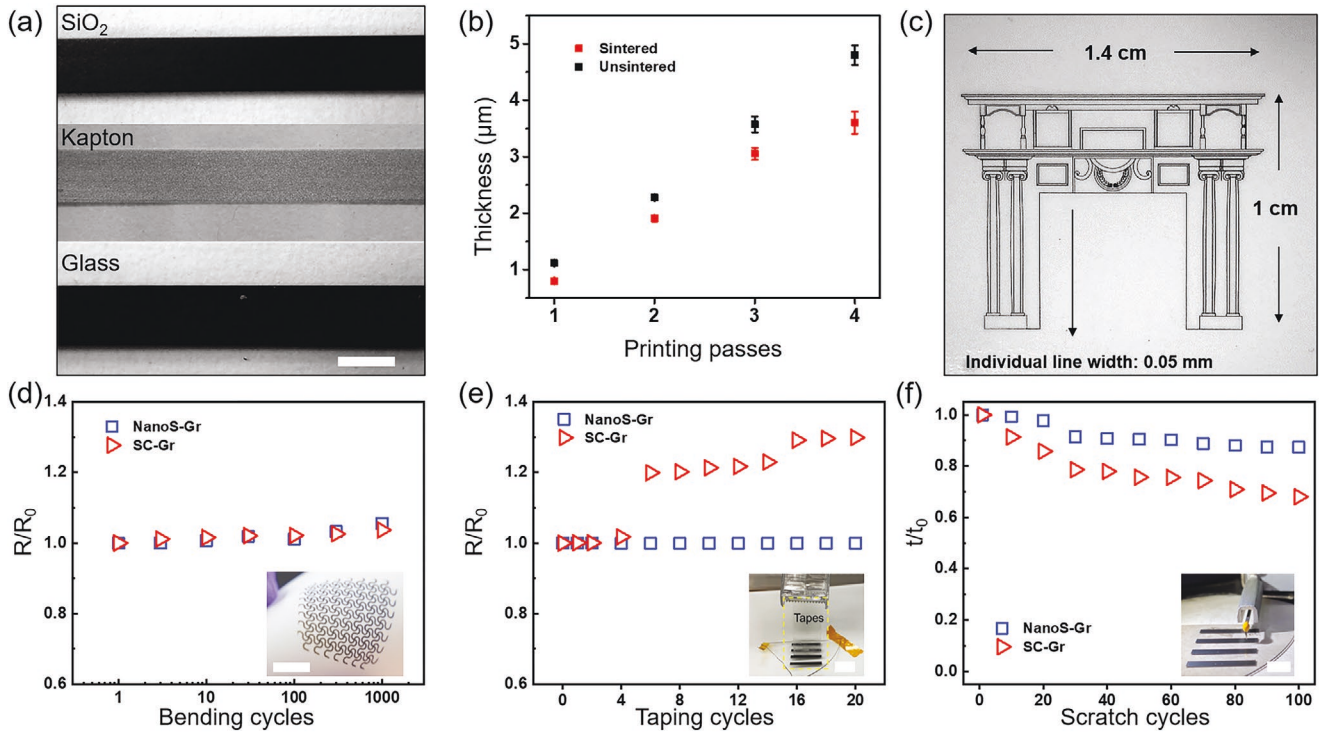

Figure 2. Printing performance of nanosurfactant-stabilized graphene inks. a) Optical microscopy images showing consistent printing of NanoS–Gr films on different substrates. Scale bar is 1 mm. b) The film thicknesses of the NanoS-stabilized graphene inks printed on Si/SiO_2 before and after annealing. c) Optical image of a printed pattern with water-based graphene ink on paper, demonstrating fine line resolution. d) Relative resistance (R/R_0) measured as a function of bending cycles for graphene films printed on polyimide substrates (bending radius of 12 mm). The inset image shows a printed serpentine pattern (scale bar: 1 cm), indicating the potential of fabricating flexible/stretchable devices. e) Resistance of graphene films versus number of tape pulling. Inset shows a graphene film under taping test with a 10 mm scale bar. f) Durability test of printed graphene films by measuring the film thickness change during 100 scratch cycles. The inset shows a NanoS–Gr film under scratching test with a tip radius of 2 µm and a scratch force of 10 mN. Scale bar in the inset is 5 mm.

to the decomposition of organic stabilizers and densification of the graphene network,[36] the NanoS remains bonded with graphene flakes after thermal annealing (200 °C) and thus the film thickness does not change significantly during this process. A scanning electron microscope (SEM) analysis (Figures S10 and S11, Supporting Information) shows the existence of small pores in the printed film with sodium cholate stabilized graphene (SC–Gr), which are likely formed due to the surfactant removal during annealing process, whereas a uniformly dense film is observed for NanoS-stabilized graphene (NanoS–Gr).

The high particle loading also allows the printing of high-resolution pattern with the use of single-pass printing (Figure 2c). To explore the possibility of applying the nanosurfactant ink for the fabrication of flexible devices, we then evaluated the structural stability of the printed NanoS–Gr film and SC–Gr film. While both films demonstrated very comparable flexibility, as indicated by negligible resistance changes during the 1000 bending cycles (Figure 2d), the NanoS–Gr film exhibited far superior robustness during the taping and scratching tests. While a 29.9% resistance increase in the SC–Gr film was observed after 20 taping cycles, the NanoS–Gr film showed negligible change in resistances even after 100 taping cycles (shown in Figure 2e and Figure S12 in the Supporting Information). Microscopic images of graphene films before and after tap pulling were recorded, as shown in Figure S13 in the Supporting Information. We found a considerable amount of graphene lost in SC–Gr films after tape pulling, while only slight changes are observed in NanoS–Gr films. This indicates that the resistance change in SC–Gr can be attributed to film damage during taping cycles. In scratching test, the NanoS–Gr film shows significantly less thickness reductions than that of the SC–Gr film after 100 scratching cycles (Figure 2f), suggesting enhanced bonding between neighboring graphene flakes due to the introduced NanoS. The improved mechanical property of NanoS–Gr is mainly attributed to the enhanced film density and interfacial bonding as a result of the NanoS sandwiched between 2D graphene flakes (Figure S11, Supporting Information). These results indicate that the NanoS not only behaves as a surfactant in ink formulation, but also serves as an interfacial bonding agent for the printed 2D flakes, eliminating the need of additional polymer binder in ink formulation.[6,19,36]

NanoS provides some unique optoelectronic properties that do not exist in the printed graphene films with conventional surfactant. The NanoS is essentially a type of semiconducting nanoparticles (Figure S1b, Supporting Information), while most molecular surfactants (e.g., SC) are organic and considered as electric insulators. As shown in **Figure 3**a, a printed pattern of NanoS showed strong photoluminescence (PL) under UV illumination. Due to the facile adsorption of semiconducting NanoS on graphene, the NanoS–based ink formulation may enable a straightforward tool to tune the bandgaps of graphene.[37] The Raman spectra of NanoS–Gr and pristine graphite in Figure 3b revealed a blue shift of the G peak in the NanoS–Gr in comparison with that of the pristine graphite, indicating a non-negligible doping effect.[38] Such doping effect was further verified using X-ray photoelectron spectroscopy

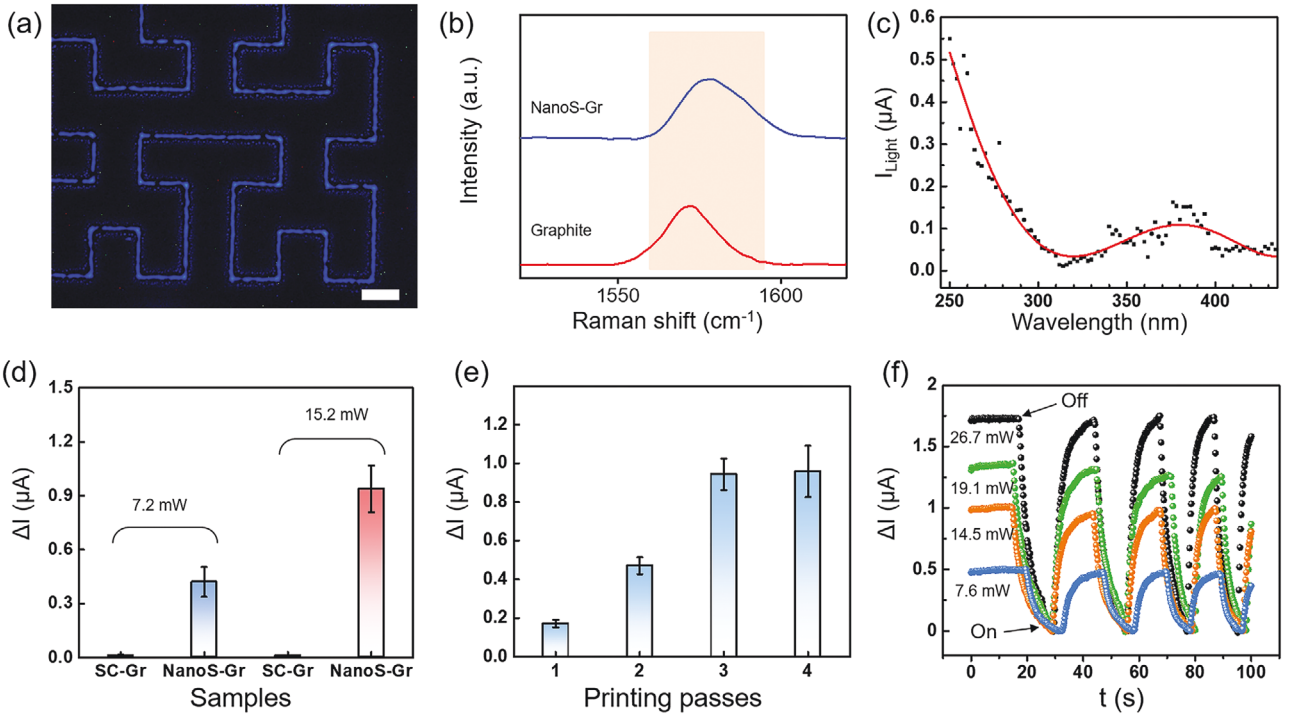

Figure 3. The optoelectronic property and spectroscopy of NanoS-stabilized graphene ink. a) Fluorescence optical microscopy image of printed QD-based nanosurfactant, showing strong photoluminescent property. Scale bar is of 200 μm. b) The Raman spectra of NanoS–Gr and graphite. c) The photocurrent of NanoS–Gr over different excitation wavelength of light. d) Photocurrent of NanoS–Gr and SC–Gr under different light powers (V_b = 2 V). Compared with SC–Gr, the NanoS–Gr showed a significantly higher photocurrent upon UV illumination. e) The photocurrent of NanoS–Gr under different printing passes. f) Current generated by switching the laser source on and off with different laser power (V_b = 2 V).

(XPS) (Figure S14, Supporting Information). The bandgap of NanoS is estimated using PL spectroscopy (Figure S14, Supporting Information),[39] revealing the photoluminescence peak for the pure NanoS at wavelengths of 463 nm (≈2.70 eV), which is similar to reported carbon-based quantum dots.[40] It is worth mentioning that the bandgaps of quantum dots are tunable depending on the particle size,[41] surface chemistry,[42] and pH values,[43] which might enable further tuning of the electronic/optical properties of GQD-based composites. The PL spectra of NanoS-stabilized graphene dispersion shows a significantly lower PL intensity than the pure NanoS, indicating a typical quenching effect induced by the adsorption of quantum dots on graphene sheets.[44] As shown in Figure 3c, the spectral photocurrent response of NanoS–Gr showed an exciton peak at around 385 nm (bias voltage (V_b) = 2.0 V), which confirms the spectral selectivity of NanoS–Gr offered by the doping effect of NanoS. It should be noted that the photocarrier generation on graphene itself is not expected to yield photoconductance because of the ultrafast recombination in graphene.[29,30] This has been confirmed by a photoconductance test of graphene with/without NanoS. As shown in Figure 3d, the generation of photocurrent ($\Delta I = I_{light} - I_{dark}$) was observed in the printed device using the NanoS–Gr ink, while the printed device using the SC–Gr ink shows no observable photocurrent. Despite similar resistivity of NanoS–Gr and SC–Gr (Table S1, Supporting Information), the significant difference in photocurrent highlights the role of NanoS particles in improving the photoconductance of graphene. The poor photoconductance of pristine graphene results from the ultrashort lifetime and fast recombination of photogenerated excitons due to graphene's gapless nature, which limits the efficient generation of photocurrent.[30,45,46] Thus, complicated device designs, such as p–n junction or Schottky junction, are often required to separate photocarriers and enhance the photocurrent.[47] An increase in UV power also results in a higher photocurrent of the NanoS–Gr device. The photocurrent of NanoS–Gr devices increases with the number of printing passes and film thicknesses before reaching a saturation point (Figure 3e), and such thickness-dependent photocurrent is also seen in GaSe photodetector.[48] Figure 3f shows the transient photocurrent responses of NanoS–Gr devices with different irradiation powers. The time response of the photocurrent decay is relatively slow (≈2 s for 50% decay at power of 26.7 mW), which is likely due to the presence of disordered interfaces in NanoS/graphene composite.[49] This undesired effect is found in other graphene composite systems, such as ZnO QDs/graphene,[50] and can be largely reduced by improving the charge transfer process from QDs to graphene under optical illumination.[51]

One of the most unique advantages of printing technology lies on the ability to rapidly convert functional nanomaterials into complex device architectures. The NanoS–Gr ink was used to print several devices with different configurations to demonstrate this rapid prototyping capability (**Figure 4**a–c; Figure S15, Supporting Information). Specifically, NanoS–Gr was incorporated with printed silver electrodes, demonstrating an all-printed in-plane photodetector (Figure 4a) as well as a cross-plane optoelectronic device (Figure 4c). NanoS–Gr inks can also be printed and incorporated along with other semiconducting materials, where an optoelectronic device of NanoS–Gr/GaN/NanoS–Gr is demonstrated (Figure 4b). Although typical *I–V* curves for the Ag/NanoS–Gr/Ag photodetectors are linear and symmetric (Ohmic contact, Figure 4d), nonlinear *I–V* curves are observed in NanoS–Gr/GaN/NanoS–Gr and cross-plane Ag/NanoS–Gr/Al devices (Figure 4e,f), indicating that there are contact barriers between NanoS–Gr and GaN as well as NanoS–Gr and Al electrodes.[52] By taking account of the UV exposed area, the normalized photocurrent densities of three types of devices are obtained (Figure S16, Supporting Information). At a bias voltage of 2 V, the cross-plane devices showed a high photocurrent of 32.1 μA and maximum photocurrent density of 458 μA cm^{-2}, which is several times higher than some reported graphene-based photodetectors,[53–56] such as CdTe- or CdSe-doped graphene systems.[53,56] The cross-plane devices demonstrated a superior performance compared with in-plane counterparts likely due to the short vertical carrier transit path, which facilitates the transport of photogenerated carriers.[57] As a proof-of-concept demonstration of developing advanced 3D sensing architectures, an array of five 3D photodetector devices is conformally printed on a hemispherical glass (radius: 15 mm.) using the NanoS–Gr as the active layer and the printed silver as the electrodes (Figure 4g). The five sensors are able to differentiate between normally incident light and obliquely incident light. When UV light is oriented such that it is normally incident on the apex of the hemispherical photodetector array (15 cm height from the reference point), the central detector exhibits a dominant photocurrent with the surrounding four detectors showing very similar photocurrents (Figure 4h). The central detector's photocurrent (91.84 μA) is almost 300% higher than that of surrounding sensors (ranging from 22.96 to 30.04 μA). However, for obliquely incident light, a considerable change in photocurrent from the sensor array is observed (Figure 4i,j), in which the most intense response emerges in the UV-light-focused photosensor (left sensor) while other sensors show much weaker photocurrent (Figure S17, Supporting Information). These results indicate that the 3D sensor array not only detects the UV light, but also provides directional information of the UV light sources. In the future, a 3D-printed UV sensor, in combination with printed visible-light or infrared sensors, may facilitate the development of next-generation bionic eyes that can realize all-angle, all-wavelength visualization.

In summary, we demonstrate an aqueous 2D material ink system that is stabilized by surface-active graphene quantum dot nanosurfactants. Thanks to the reduced interfacial tension of inks enabled by nanosurfactants, the aqueous dispersions of graphene, MoS_2, WS_2, and h-BN nanosheets are colloidally stable and can be readily used in printing processes. Similar to small-molecule surfactants, the nanosurfactant-based printing technique enables rapid fabrication of complex device structures with high spatial resolution. More importantly, nanosurfactants not only eliminates the prerequisite of thermal treatment for the removal of organic surfactants, but also becomes an integrated part of the printed device and results in unique functionalities and superior performances in printed 2D-crystal-based devices, including bandgap engineering, enhanced photoconductance of ink materials, and improved film robustness. The research offers a facile, versatile, and highly scalable approach of printing 2D nanomaterials into functional devices, which is

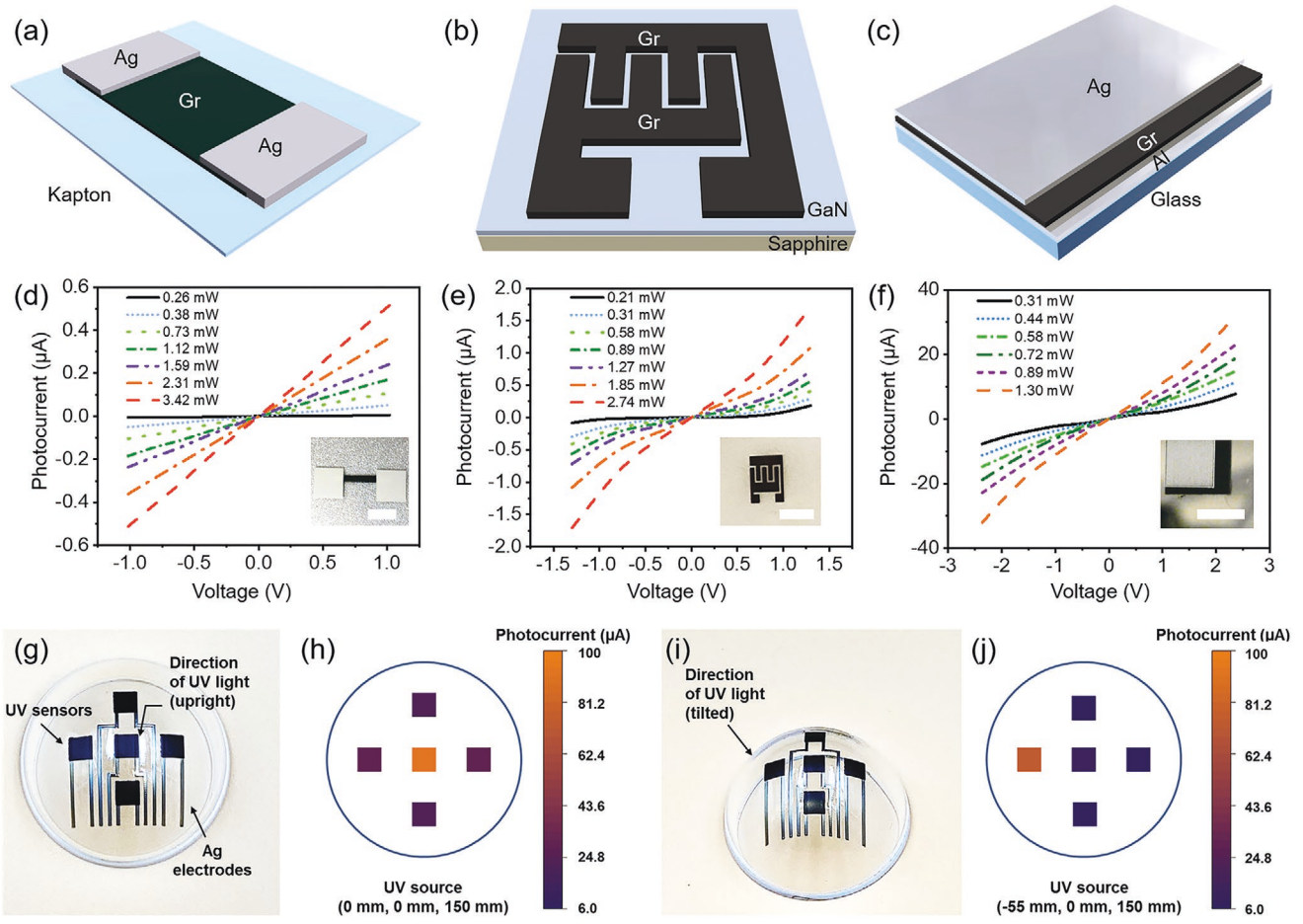

Figure 4. Printed UV sensors on 2D and 3D substrates using NanoS–Gr ink. a–c) Schematic illustrations of in-plane device of Ag/NanoS–Gr/Ag (a) and NanoS–Gr/GaN/NanoS–Gr (b), and of a cross-plane device of Ag/NanoS–Gr/Al (c). d–f) The *I*–*V* curves corresponding to the three photodetectors under UV illumination shown in (a)–(c), respectively. The insets of (d)–(f) are camera images of the printed devices with scale bars of 5, 5, and 3 mm, respectively. g) Photographic image of all-printed 3D photodetector array and h) the photocurrent mapping under upright illumination. i) Photographic image of all-printed 3D photodetector array and j) the photocurrent mapping under tilted-angle illumination. The radius of hemisphere is 15 mm.

expected to find broad applications in sensors, energy conversion/storage devices, and flexible and wearable electronics.

Experimental Section

Synthesis of NanoS: Graphene quantum dot nanosurfactant was prepared following a reported work.[28] First, citric acid (1.4 g) and sodium *p*-styrenesulfonate (0.6 g) were fully homogenized using a vortex machine. Then, the above mixture was loaded in a 20 mL glass vial followed by calcination in air at 200 °C for 80 min. After the system cooled down to room temperature, 5 mL deionized water was used to fully dissolve dark solid residue, followed by a dialysis treatment (2000 Da) to separate unreacted starting materials and byproducts. The final product was dried under vacuum before being diluted into desired concentration for the exfoliation experiments.

Preparation of Graphene, CNT, and Other 2D Crystal Inks: For the synthesis of 1D/2D crystal ink, GQD was used as nanosurfactants. Taking graphene ink for example, 1 g of nanosurfactant was dissolved in deionized water to obtain a 20 mg mL^{-1} nanosurfactant solution (50 mL). Then, 2 g of graphite (Asbury Carbons, grade 3805) was added into the above solution and was tip-sonicated for 1 h. The as-prepared sonicated product was centrifuged at 2000 rpm for 30 min to remove unexfoliated bulk crystals. For graphene ink stabilized by a small-molecule surfactant, sodium cholate was used to replace nanosurfactant while other experimental details remained the same.

3D Aerosol Jet Printing: A high-resolution aerosol jet printer (OPTOMEC AJP 300) was employed to print nanomaterial inks with a printing speed from 3 to 21 mm s^{-1}. Computer-aided design software (AutoCAD) was used to generate printable patterns for the device fabrication. Additional printing parameters and details can be found in the Supporting Information.

Characterization: The colloidal stability of nanomaterial inks was evaluated by zeta potential measurements (Nano-ZS, Malvern, USA). A transmission electron microscope (JEOL 2011, Japan) was used to image the 2D flakes as well as the nanosurfactants. A focused ion beam-scanning electron microscope (FIB-SEM, Helios G4 UX) was used to obtain SEM images of samples. Fluorescence microscopy images were taken using a Nikon Eclipse 90i Widefield Fluorescent Microscope. The flexibility of the film was studied using repeated bending testing with bending radius of 12 mm (≈90°). Adhesive tapes (3M Scotch Double Sided Removable Tape, USA) were used to evaluate the mechanical robustness of printed graphene films with a metal object of 50 g, which was used to apply a constant pressure (≈20 KPa) on tapes for ensuring the good contact between adhesive tape and graphene film. The scratching experiments were performed using a stylus profilometer (Bruker Corporation, USA) with a tip radius of 2 μm and a stylus force of 10 mN (≈795.8 MPa).

Supporting Information

Supporting Information is available from the Wiley Online Library or from the author.

Acknowledgements

Y.Z. would like to acknowledge funding support from the National Science Foundation under award CMMI-1747685, and the U.S. Department of Energy under awards DE-NE0008712 and DE-NE0008701. Z.C. would like to acknowledge support by NASA under the grant NNX13AQ60G. The authors thank Notre Dame Integrated Imaging Facility and Materials Characterization Facility for assistance in material characterization.

Conflict of Interest

The authors declare no conflict of interest.

Keywords

2D materials, 3D conformal printing, colloidal inks, nanosurfactants

Received: May 6, 2020
Revised: July 20, 2020
Published online:

[1] Z. Lin, Y. Liu, U. Halim, M. Ding, Y. Liu, Y. Wang, C. Jia, P. Chen, X. Duan, C. Wang, F. Song, M. Li, C. Wan, Y. Huang, X. Duan, *Nature* **2018**, *562*, 254.
[2] M. S. Saleh, C. Hu, R. Panat, *Sci. Adv.* **2017**, *3*, e1601986.
[3] D. Katerinopoulou, P. Zalar, J. Sweelssen, G. Kiriakidis, C. Rentrop, P. Groen, G. H. Gelinck, J. van den Brand, E. C. P. Smits, *Adv. Electron. Mater.* **2019**, *5*, 1800605.
[4] M. Saeidi-Javash, W. Kuang, C. Dun, Y. Zhang, *Adv. Funct. Mater.* **2019**, *29*, 1901930.
[5] W. J. Hyun, E. B. Secor, C.-H. Kim, M. C. Hersam, L. F. Francis, C. D. Frisbie, *Adv. Energy Mater.* **2017**, *7*, 1700285.
[6] M. Zeng, Y. Zhang, *J. Mater. Chem. A* **2019**, *7*, 23301.
[7] A. Shinde, D. Huang, M. Saldivar, H. Xu, M. Zeng, U. Okeibunor, L. Wang, C. Mejia, P. Tin, S. George, L. Zhang, Z. Cheng, *ACS Nano* **2019**, *13*, 12461.
[8] M. Zeng, D. King, D. Huang, C. Do, L. Wang, M. Chen, S. Lei, P. Lin, Y. Chen, Z. Cheng, *Proc. Natl. Acad. Sci. USA* **2019**, *116*, 18322.
[9] M. Chen, A. Shinde, L. Wang, C. Ye, M. Zeng, Q. Yan, P. Lin, Y. Chen, Z. Cheng, *2D Mater.* **2019**, *6*, 025031.
[10] A. G. Kelly, T. Hallam, C. Backes, A. Harvey, A. S. Esmaeily, I. Godwin, J. Coelho, V. Nicolosi, J. Lauth, A. Kulkarni, S. Kinge, L. D. Siebbeles, G. S. Duesberg, J. N. Coleman, *Science* **2017**, *356*, 69.
[11] A. Gupta, V. Arunachalam, S. Vasudevan, *J. Phys. Chem. Lett.* **2015**, *6*, 739.
[12] J. N. Coleman, *Adv. Funct. Mater.* **2009**, *19*, 3680.
[13] R. J. Smith, P. J. King, M. Lotya, C. Wirtz, U. Khan, S. De, A. O'Neill, G. S. Duesberg, J. C. Grunlan, G. Moriarty, J. Chen, J. Wang, A. I. Minett, V. Nicolosi, J. N. Coleman, *Adv. Mater.* **2011**, *23*, 3944.
[14] S. Lu, J. A. Cardenas, R. Worsley, N. X. Williams, J. B. Andrews, C. Casiraghi, A. D. Franklin, *ACS Nano* **2019**, *13*, 11263.
[15] D. McManus, S. Vranic, F. Withers, V. Sanchez-Romaguera, M. Macucci, H. Yang, R. Sorrentino, K. Parvez, S.-K. Son, G. Iannaccone, K. Kostarelos, G. Fiori, C. Casiraghi, *Nat. Nanotechnol.* **2017**, *12*, 343.
[16] S. Nakata, T. Arie, S. Akita, K. Takei, *ACS Sens.* **2017**, *2*, 443.
[17] T. Varghese, C. Hollar, J. Richardson, N. Kempf, C. Han, P. Gamarachchi, D. Estrada, R. J. Mehta, Y. Zhang, *Sci. Rep.* **2016**, *6*, 33135.
[18] S. Agarwala, G. L. Goh, T.-S. Dinh Le, J. An, Z. K. Peh, W. Y. Yeong, Y.-J. Kim, *ACS Sens.* **2019**, *4*, 218.
[19] E. B. Secor, B. Y. Ahn, T. Z. Gao, J. A. Lewis, M. C. Hersam, *Adv. Mater.* **2015**, *27*, 6683.
[20] P. Lin, Q. Yan, Y. Chen, X. Li, Z. Cheng, *Chem. Eng. J.* **2018**, *334*, 1023.
[21] Z. Yang, J. Wei, Y. I. Sobolev, B. A. Grzybowski, *Nature* **2018**, *553*, 313.
[22] X. Wang, M. Zeng, Y.-H. Yu, H. Wang, M. S. Mannan, Z. Cheng, *ACS Appl. Mater. Interfaces* **2017**, *9*, 7852.
[23] Y.-H. Yu, Y.-P. Chen, M. Zeng, Z. Cheng, *Mater. Lett.* **2016**, *163*, 158.
[24] D. Luo, F. Wang, J. Zhu, F. Cao, Y. Liu, X. Li, R. C. Willson, Z. Yang, C.-W. Chu, Z. Ren, *Proc. Natl. Acad. Sci. USA* **2016**, *113*, 7711.
[25] I. Raj, M. Qu, L. Xiao, J. Hou, Y. Li, T. Liang, T. Yang, M. Zhao, *Fuel* **2019**, *251*, 514.
[26] J. Luo, M. Zeng, B. Peng, Y. Tang, L. Zhang, P. Wang, L. He, D. Huang, L. Wang, X. Wang, M. Chen, S. Lei, P. Lin, Y. Chen, Z. Cheng, *Angew. Chem., Int. Ed.* **2018**, *57*, 11752.
[27] L. Zhang, Q. Lei, J. Luo, M. Zeng, L. Wang, D. Huang, X. Wang, S. Mannan, B. Peng, Z. Cheng, *Sci. Rep.* **2019**, *9*, 163.
[28] M. Zeng, S. A. Shah, D. Huang, D. Parviz, Y.-H. Yu, X. Wang, M. J. Green, Z. Cheng, *ACS Appl. Mater. Interfaces* **2017**, *9*, 30797.
[29] P. A. George, J. Strait, J. Dawlaty, S. Shivaraman, M. Chandrashekhar, F. Rana, M. G. Spencer, *Nano Lett.* **2008**, *8*, 4248.
[30] G. Konstantatos, M. Badioli, L. Gaudreau, J. Osmond, M. Bernechea, F. P. G. de Arquer, F. Gatti, F. H. L. Koppens, *Nat. Nanotechnol.* **2012**, *7*, 363.
[31] D. Parviz, S. Das, H. S. T. Ahmed, F. Irin, S. Bhattacharia, M. J. Green, *ACS Nano* **2012**, *6*, 8857.
[32] A. Schlierf, H. Yang, E. Gebremedhn, E. Treossi, L. Ortolani, L. Chen, A. Minoia, V. Morandi, P. Samori, C. Casiraghi, *Nanoscale* **2013**, *5*, 4205.
[33] H. Yang, F. Withers, E. Gebremedhn, E. Lewis, L. Britnell, A. Felten, V. Palermo, S. Haigh, D. Beljonne, C. Casiraghi, *2D Mater.* **2014**, *1*, 011012.
[34] E. B. Secor, P. L. Prabhumirashi, K. Puntambekar, M. L. Geier, M. C. Hersam, *J. Phys. Chem. Lett.* **2013**, *4*, 1347.
[35] J. Li, F. Ye, S. Vaziri, M. Muhammed, M. C. Lemme, M. Östling, *Adv. Mater.* **2013**, *25*, 3985.
[36] E. B. Secor, S. Lim, H. Zhang, C. D. Frisbie, L. F. Francis, M. C. Hersam, *Adv. Mater.* **2014**, *26*, 4533.
[37] A. E. Mansour, M. M. Said, S. Dey, H. Hu, S. Zhang, R. Munir, Y. Zhang, K. Moudgil, S. Barlow, S. R. Marder, A. Amassian, *Adv. Funct. Mater.* **2017**, *27*, 1602004.
[38] J.-B. Wu, M.-L. Lin, X. Cong, H.-N. Liu, P.-H. Tan, *Chem. Soc. Rev.* **2018**, *47*, 1822.
[39] D. I. Son, B. W. Kwon, D. H. Park, W.-S. Seo, Y. Yi, B. Angadi, C.-L. Lee, W. K. Choi, *Nat. Nanotechnol.* **2012**, *7*, 465.
[40] H. Yoon, Y. H. Chang, S. H. Song, E.-S. Lee, S. H. Jin, C. Park, J. Lee, B. H. Kim, H. J. Kang, Y.-H. Kim, S. Jeon, *Adv. Mater.* **2016**, *28*, 5255.
[41] X. Yan, B. Li, X. Cui, Q. Wei, K. Tajima, L.-S. Li, *J. Phys. Chem. Lett.* **2011**, *2*, 1119.
[42] M. A. Sk, A. Ananthanarayanan, L. Huang, K. H. Lim, P. Chen, *J. Mater. Chem. C* **2014**, *2*, 6954.
[43] C. Zhu, S. Yang, G. Wang, R. Mo, P. He, J. Sun, Z. Di, N. Yuan, J. Ding, G. Ding, X. Xie, *J. Mater. Chem. C* **2015**, *3*, 8810.
[44] C. Anichini, W. Czepa, D. Pakulski, A. Aliprandi, A. Ciesielski, P. Samorì, *Chem. Soc. Rev.* **2018**, *47*, 4860.

[45] F. Xia, T. Mueller, Y.-m. Lin, A. Valdes-Garcia, P. Avouris, *Nat. Nanotechnol.* **2009**, *4*, 839.
[46] W. Bao, L. Jing, J. Velasco, Y. Lee, G. Liu, D. Tran, B. Standley, M. Aykol, S. B. Cronin, D. Smirnov, M. Koshino, E. McCann, M. Bockrath, C. N. Lau, *Nat. Phys.* **2011**, *7*, 948.
[47] C. Xie, Y. Wang, Z.-X. Zhang, D. Wang, L.-B. Luo, *Nano Today* **2018**, *19*, 41.
[48] P. J. Ko, A. Abderrahmane, T. Takamura, N.-H. Kim, A. Sandhu, *Nanotechnology* **2016**, *27*, 325202.
[49] P. Fantuzzi, A. Candini, Q. Chen, X. Yao, T. Dumslaff, N. Mishra, C. Coletti, K. Müllen, A. Narita, M. Affronte, *J. Phys. Chem. C* **2019**, *123*, 26490.
[50] H. Chang, Z. Sun, K. Y.-F. Ho, X. Tao, F. Yan, W.-M. Kwok, Z. Zheng, *Nanoscale* **2011**, *3*, 258.
[51] Z. Sun, Z. Liu, J. Li, G.-A. Tai, S.-P. Lau, F. Yan, *Adv. Mater.* **2012**, *24*, 5878.
[52] C. Zhang, S. Wang, L. Yang, Y. Liu, T. Xu, Z. Ning, A. Zak, Z. Zhang, R. Tenne, Q. Chen, *Appl. Phys. Lett.* **2012**, *100*, 243101.
[53] Z. Tao, Y.-A. Huang, X. Liu, J. Chen, W. Lei, X. Wang, L. Pan, J. Pan, Q. Huang, Z. Zhang, *Nano-Micro Lett.* **2016**, *8*, 247.
[54] R.-J. Shiue, Y. Gao, Y. Wang, C. Peng, A. D. Robertson, D. K. Efetov, S. Assefa, F. H. L. Koppens, J. Hone, D. Englund, *Nano Lett.* **2015**, *15*, 7288.
[55] Y. Wang, C.-W. Ge, Y.-F. Zou, R. Lu, K. Zheng, T.-F. Zhang, Y.-Q. Yu, L.-B. Luo, *Adv. Opt. Mater.* **2016**, *4*, 291.
[56] G. Yang, D. Kim, J. Kim, *Opt. Express* **2015**, *23*, A1081.
[57] H.-C. Cheng, G. Wang, D. Li, Q. He, A. Yin, Y. Liu, H. Wu, M. Ding, Y. Huang, X. Duan, *Nano Lett.* **2016**, *16*, 367.